

The thermal effect on electrical capacitance sensor for two-phase flow monitoring

Wael A. Altabey^{*1,2}

¹International Institute for Urban Systems Engineering, Southeast University, Nanjing (210096), China

²Department of Mechanical Engineering, Faculty of Engineering, Alexandria University, Alexandria (21544), Egypt

(Received June 8, 2016, Revised September 10, 2016, Accepted September 13, 2016)

Abstract. One of major errors in flow rate measurement for two-phase flow using an Electrical Capacitance Sensor (ECS) concerns sensor sensitivity under temperature raise. The thermal effect on electrical capacitance sensor (ECS) system for air–water two-phase flow monitoring include sensor sensitivity, capacitance measurements, capacitance change and node potential distribution is reported in this paper. The rules of 12-electrode sensor parameters such as capacitance, capacitance change, and change rate of capacitance and sensitivity map the basis of Air–water two-phase flow permittivity distribution and temperature raise are discussed by ANSYS and MATLAB, which are combined to simulate sensor characteristic. The cross-sectional void fraction as a function of temperature is determined from the scripting capabilities in ANSYS simulation. The results show that the temperature raise had a detrimental effect on the electrodes sensitivity and sensitive domain of electrodes. The FE results are in excellent agreement with an experimental result available in the literature, thus validating the accuracy and reliability of the proposed flow rate measurement system.

Keywords: electrical capacitance sensor (ECS); thermal effect; two-phase flow monitoring; finite element method

1. Introduction

The flow regimes and the void fraction are important parameters to describe two-phase flow, and measurement of two-phase flow parameters is becoming increasingly important in many industrial processes such as physical, chemical and petroleum industrial processes. On-line measurement of two-phase flow parameters not only helps analyze the effect of the flow pattern on phase fraction and flow rate measurement but also plays an important role in the safety of operation and the reliability of practical processes (Hetsroni 1982, Thorn, Johansen *et al.* 1997, Thorn, Johansen *et al.* 1999).

In order to achieve even more voracious measurement information on two-phase pipe flow section, and carry out non-touch and non-disturbance collecting information, many novel sensor

*Corresponding author, Assistant Professor, E-mail: wael.altabey@gmail.com

¹ Current Affiliation

² Previous Affiliation

techniques have been applied to the measurement of two-phase flow, such as radiation (Banerjee and Lahey 1981), laser (Kumar, Cook *et al.* 1995), nuclear magnetic resonance (NMR) (Lynch and Segal 1977) and ultrasonics (Couthard and Yan 1993).

One kind of attractive technique to measure two-phase flow parameters is a method uses non-intrusive or sensors that are located on the periphery of objects, such as process vessels or pipelines, to reconstruct the spatial distribution of the interfaces among various phases, i.e. the dielectric constant (or relative permittivity) inside the sensor area and then form the cross-sectional image of the phase distributions of objects.

The electrical Capacitance sensor (ECS) was first introduced in the 1980s by a group of researchers from the US Department of Energy Morgantown Energy Technology Center (METC), to measure fluidized bed system (Fasching and Smith 1988, Fasching and Smith 1991, Huang *et al.* 1989). The technique have been developed rapidly during the past 10 years, and then they have become popular and gained importance to monitor industrial processes due to its low cost and its operability under harsh environmental conditions.

The accurate of two-phase flow measurement technologies present practical challenges and continued progress is being made toward improving these technologies. Therefore, the area of ECS sensitivity improved to increase the accuracy of two-phase flow measurements has been an intensive research topic for several decades.

The need for a more accurate measurement of ECS led to the study of the factors which have influence and effect on ECS sensitivity and sensitive domain of ECS electrodes. There are three factors have been studied and found which have effect on ECS measurements, e.g., pipeline material, inner dielectric permittivity (Jaworski and Bolton 2000, Pei and Wang 2009, Al-Tabey 2010, Asencio, Bramer-Escamilla *et al.* 2015, Sardeshpande, Harinarayan *et al.* 2015, Mohamad, Rahim *et al.* 2016) and the ratio of pipeline thickness and diameter (Daoye, Bin *et al.* 2009, Altabay 2016).

The objective of this paper is to study a new factor has a great influence and effect on ECS sensitivity and sensitive domain of ECS electrodes, in order to increase the accuracy of two-phase flow measurements. This factor is the temperature raise of fluid flow and pipe wall due to the hot weather in the several countries, and that causes the difference between the real void fraction and the measured one from ECS. The simulation results are obtained using ANSYS and MATLAB software. The results show the excellent agreement between FE results and experimental results available in the literature, thus validating the accuracy and reliability of the proposed study.

2. Electrical capacitance sensor (ECS)

ECS is one of the most mature and promising methods, which measures the capacitance change of multi-electrode sensor due to the change of dielectric permittivity being imaged, and then reconstructs the cross-section images using the measured raw data with a suitable algorithm. It has the characteristics such as low cost, fast response, non-intrusive method, broad application, safety (Yang *et al.* 1995a, b, Li and Huang 2000, Mohamad, Rahim *et al.* 2012 and Zhang, Wang *et al.* 2014). Electrical capacitance system includes sensor, capacitance measuring circuit and imaging computer is shown in Fig. 1. And ECS consists of insulating pipe, measurement electrode, radial screen and earthed screen (Yang and York 1999). The measurement electrode is mounted symmetrically around the circumference of pipeline. Radial screen is fitted between the electrodes to cut the electroline external to the sensor pipeline and reduce the inter-electrode capacitance. The

earthed screen surrounds the measurement electrodes to shield external electromagnetic noise. ECS converts the permittivity of inner media flow to inter-electrode capacitance, which is the ECS forward problem. Capacitance measuring circuit takes the capacitance data and transfers to imaging computer. Imaging computer reconstructs the distribution image with a suitable algorithm, which is called ECS inverse problem. In most application, ECS electrode is mounted outside the pipeline which is called external electrode ECS (Yang 1997).

2.1 The ECS geometrical model

The model section comprises of an ECT sensor column with 0.1 m inner diameter and 0.3 m height. The ECT sensor is made up of Perspex material and having a ring of 12 electrodes (which are separated from each other by small gap) on its outer periphery. Fig. 2 shows the cross section of 12-electrode ECS system, in which R_1 is inner pipe radius; R_2 is outer pipe radius; R_3 is earthed screen radius.

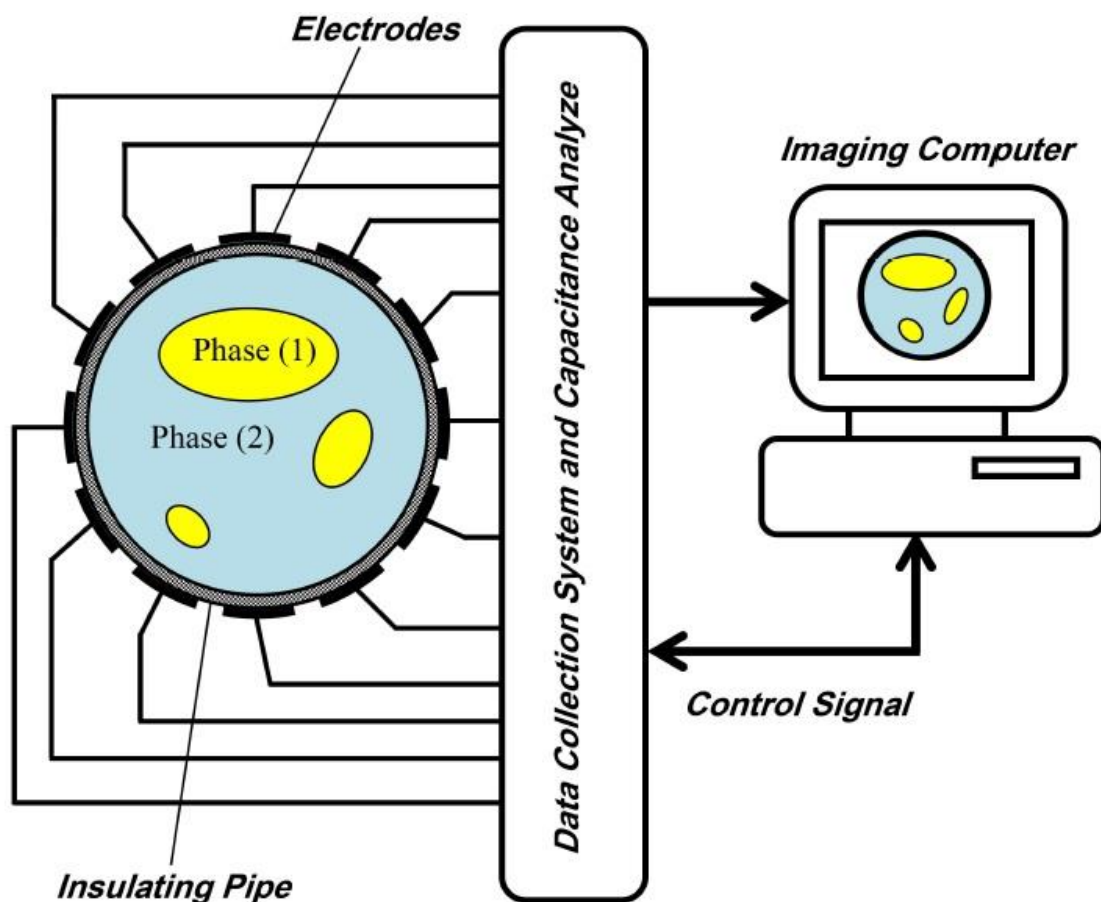


Fig. 1 Sketch of ECS system

The ECS also includes radial guard electrodes to constrain the field lines from the excited electrode and reduce the dependence of spacing between the electrodes and the screen as shown in the Figure. The function of the sensor includes measuring the capacitance between all possible combination pairs of the electrodes and converting the measured capacitance values in to the voltage signals. The water is supplied from a pump inside the vertical Perspex pipe, and the compressed air is pumped through the pipe and enters the sensor from the bottom. The water also flows into bottom part of ECS and mixed with the compressed air to generate bubbles before entering the sensing section of the sensor. The different bubbles size and locations are modeled to simulate the effect of air–water two-phase flow. We will get the distribution of electric sensitive potential and media distribution on the sensitive field. The permittivity values of Perspex, water and air are 3.0, 80 and 1.0 respectively. There are 12 set excitation electrodes and the excitation voltage is 15 volts, the sensors physical specification are shown in Table 1.

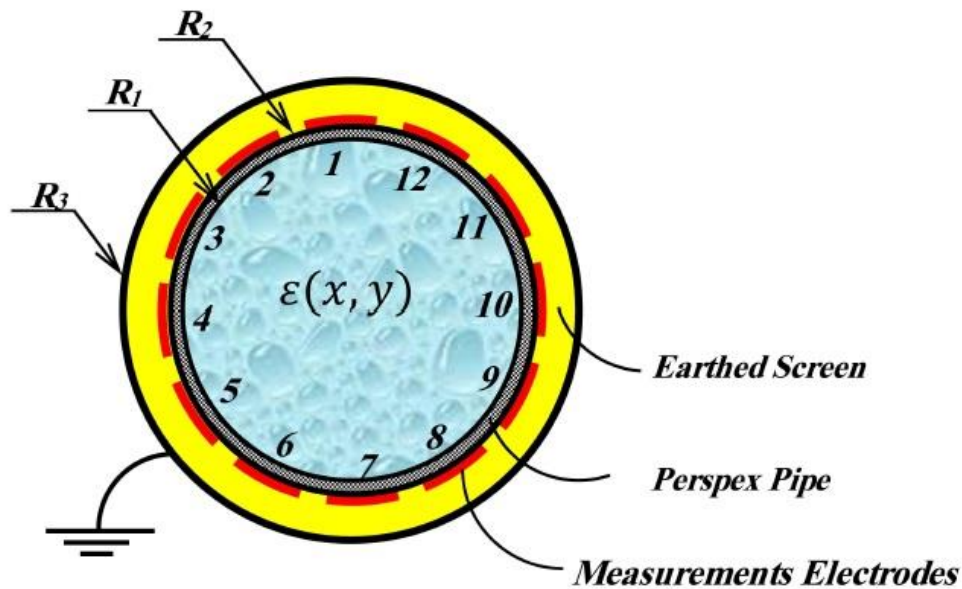


Fig. 2 Cross section sketch of 12-electrode ECS

Table 1 Sensor physical specification

ECS system	Specification
No. of electrodes	12
Space between electrodes	2 mm
Inner/outer pipe diameter	94/100 mm
Earth Screen diameter	110 mm
Thickness of electrodes	1mm
End guards	50 mm
Permittivity pipe wall/ Water/ Air	$\epsilon_r = 3/ \epsilon_w = 80/ \epsilon_A = 1.0$
Excitation voltage	$\phi = 15$ Volts

2.2 The ECS composition and working principle

For 12-electrode system, the electrodes are numbered as shown in the Fig. 3, are excited with an electric potential, one at a time in increasing order, when one electrode is excited, the other electrodes are kept at ground potential as shown in the Fig. 3 and act as detector electrodes. When electrode No. 1 is excited with a potential, the charge $Q_{1,j}$ is induced on the electrodes, $j = 2, \dots, N$ can be measured. Next, electrode No. 2 is excited whereas, rest the electrodes are kept at ground potential, and the induced charges $Q_{2,3}, Q_{2,4}, \dots, Q_{2,N}$ ($N = 12$) are measured. The measurement protocol continues until electrode $N - 1$ is excited. Using these charge measurements, the inter electrode capacitance C_{ij} can be computed using the definition of capacitance in Eq. (1)

$$C_{ij} = \frac{Q_{ij}}{\Delta V_{ij}} \tag{1}$$

Where Q_{ij} is the charge induced on electrode j when electrode i is excited with a known potential. V_{ij} is the potential difference between electrodes i and j ($\Delta V_{ij} = V_i - V_j$). So the number of independent capacitance measurements $M = 66$ using Eq. (2) is

$$M = \frac{N(N-1)}{2} \tag{2}$$

It is important to note that these capacitances are dependent on the geometry of electrodes and the determined once size and location of the electrodes and the permittivity distribution $\epsilon(x,y)$ are known. A change in the permittivity distribution $\epsilon(x,y)$ is naturally reflected in the capacitance measurements. The actual capacitance changes measured will be very small, in the order of Pico or Femto Farad ($10^{-12}F$ or $10^{-15}F$). Sequential electrodes are referred to as adjacent electrodes; have the largest standing capacitance, while diagonally or opposing electrodes will have the smallest capacitances.

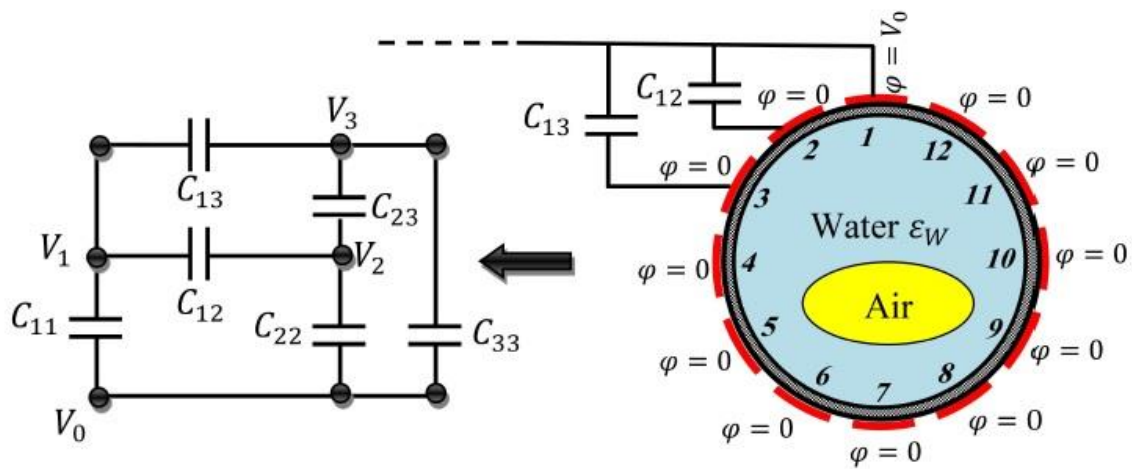


Fig. 3 Schematic representation of the measurement principle of an ECS

3. Finite element simulation model

In terms of Electrical Capacitance sensor (ECS), the forward problem is the problem of calculating the capacitance matrix C from a given set of sensor design parameters and a given cross-sectional permittivity ε .

The forward model proposed for ECS (Xie, Huang *et al.* 1992) is based on finite element simulations. It is assumed that both the flow distribution and the electrical field during the measurement set are 2D and static. Changes in axial direction are neglected within the axial electrode length. Furthermore free charges in the flow are also neglected. Thus, the system obeys the following Poisson equation

$$\nabla \cdot \varepsilon(x, y) \nabla \varphi(x, y) = 0 \quad (3)$$

The 2D models considered in this study were constructed using commercially available finite element software, ANSYS (The Electrostatic Module in the Electromagnetic subsection of ANSYS (2014), Al-Tabey 2012). The problem space was divided into triangular elements. In a region of ideal dielectrics and space charges, the potential $\varphi(x, y)$ inside the ECS is determined by solving the Poisson's equation. For the boundary condition imposed on the ECS head by the measurement system, the potential $\varphi(x, y)$ can be found. The electric field vector $E(x, y)$, the electric flux density $D(x, y)$ and the potential function $\varphi(x, y)$ are related as follows

$$E(x, y) = -\nabla \varphi(x, y) \quad (4)$$

$$D = \varepsilon(x, y) E(x, y) \quad (5)$$

The change on the electrodes, and hence the inter electrode capacitances for each electrode pairs that reward the value of the permittivity can be found by using the definition of the capacitance in Eq. (1), and substitute it in Gauss's law based on the following surface integral

$$Q_{ij} = \oint_{S_j} (\varepsilon(x, y) \nabla \varphi(x, y) \cdot \hat{n}) ds \quad (6)$$

Where: $\varepsilon(x, y)$ is permittivity, $\nabla \cdot$ is divergence operator, ∇ is gradient operator, S_j is a surface enclosing electrode j , ds is an infinitesimal area on electrode j , \hat{n} is the unit vector normal to S_j and ds is an infinitesimal area on it.

3.1 The boundary conditions

The potential boundary conditions were applied to the sensor-plate (electrodes). For one electrode, the boundary condition of electric potential ($V=V_0$) with 15 V (V_0) was applied and another electrode was kept at ground ($V=0$) potential to simulate a 15 V (RMS) potential gradient across the electrodes. For representing the natural propagation of electric field, the default boundary condition of continuity ($\hat{n} \cdot (D_1 - D_2) = 0$) was maintained for the internal boundaries.

3.2 The field partition

According to finite element analysis, we will carry out imaging of regional triangulation, it is necessary to divided pixel pipe into triangular finite element, because many pipes are round under

the circumstances of a smaller number of pixels, we can achieve higher accuracy to use the triangle mesh than rectangular grids, To improve the accuracy of mesh, we will take subdivision method two times imaging region is divided into 4388 Elements. To improve the accuracy of mesh, we divided the meshed region again into 8884 Elements; the map is as follows in Fig. 4.

4. Results and discussions

4.1 Air–water two-phase flow measurement ditection

Some of dataset used in this presented model is adapted from the experimental work of Alme and Mylvaganam (2006). The approach taken by ANSYS 2D is to divide the different materials and geometries into triangular elements as shown in Fig. 4, and to represent the electric field (see Eq. (4)) within each element with a separate polynomial. The software only computes the potential and the electric field values at the element nodes and interpolate between these nodes to obtain the values for other points within the elements.

The Air–Water two-phase flow measurements for the ANSYS 2D simulation, when electrode 7 is excited, are illustrated in Fig. 5. Where five cylindrical bubble of air have a different in diameter, surrounded by water has the relative permittivity $\epsilon_w = 80$, the first bubble has 40 mm dia., is located at coordinates $x = 0$ mm and $y = -17$ at time 1 (Alme and Mylvaganam 2006), the second bubble has 42.5 mm dia., is located at $x = -10$ mm and $y = -5$ at time 2, the third bubble has 45mm dia., is located at $x = 0$ mm and $y = 5$ at time 3, the fourth bubble has 47.5mm dia., is located at $x = 5$ mm and $y = 5$ at time 4 and final bubble has 50mm dia., is located at $x = 0$ mm and $y = 0$ at time 5, respectively, with constant working conditions, water pressure ($\Delta P = 10$ MPa) and room temperature 25°C. And then the outer surface of the pipe wall temperature is increased to 60°C and the inner surface of the pipe still at room temperature 25°C, with heat convection coefficient between the pipe wall and water is $h = 10 W/(m^2 \cdot ^\circ C)$.

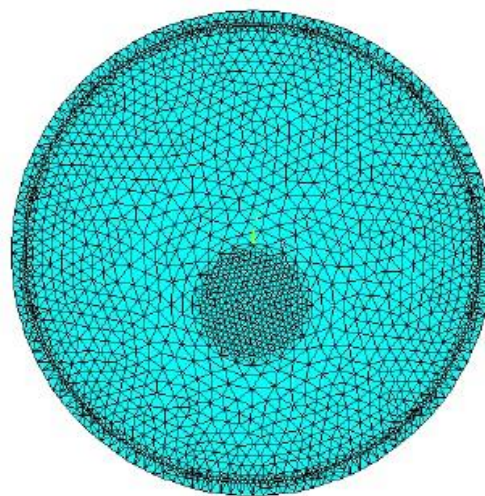


Fig. 4 (8884) Element map of finite element mesh

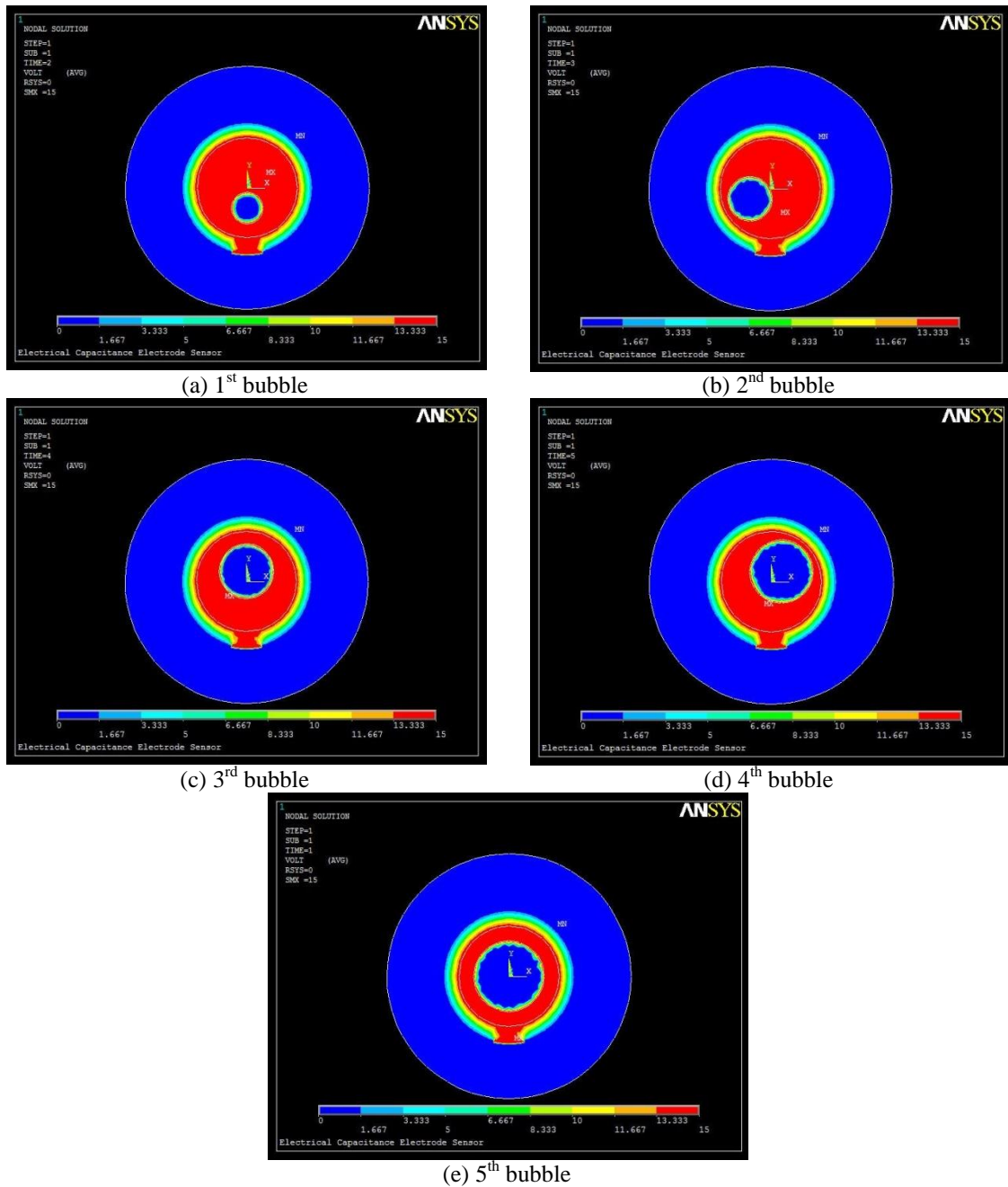


Fig. 5 node potential equivalent of Air–Water two-phase flow measurements from ANSYS 2D model

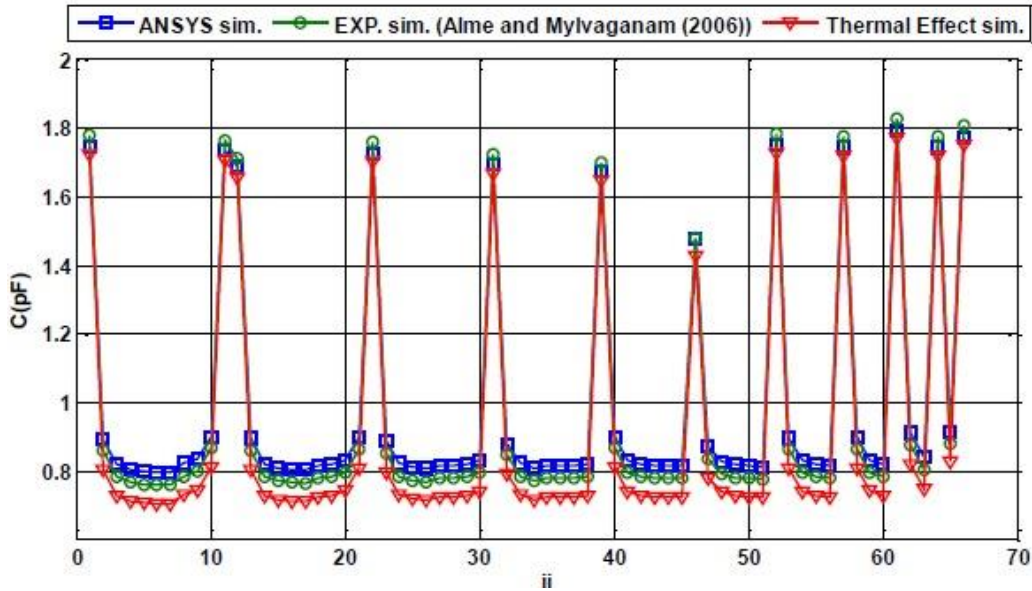


Fig. 6 Comparison of simulated capacitances from 2D ANSYS model for Air–Water two-phase flow between the 2D ANSYS model and experimental model at room temperature and with thermal effect.

Fig. 6 shows the comparison of 66 capacitance measurements (M) of Air–Water two-phase flow between the 2D ANSYS model and (Alme and Mylvaganam 2006) model at room temperature and with thermal effect.

From these Fig. we can be seen the excellent agreement between the finite element and experimental data with an average error of 0.925%. The deviation between the experimental and finite element data is due to the fact that the 2D finite element simulations ignore the fringe-field effects at the outer edges of the electrodes.

Fig. 7 shows the sensor sensitivity versus the bubble No., the sensor sensitivity is defined as

$$Sensor\ sensitivity\% = \frac{C_h - C_l}{C_l} \times 100 \tag{7}$$

Where C_h and C_l are the capacitance measurements for high and low temperature cases respectively.

The sensor sensitivity decreases with the increase in the pipe wall temperature as the sensor has a sensitivity ranging between 4.569 and 1.19% for temperature (T) ranging between 25 and 60 °C for selected sensor geometrical parameters.

Using the exponential formula (8) to fit the sensor sensitivity have proved its suitability by giving acceptable values for the correlation factor (C.F) is 0.9398 are very near to unity.

$$Sensor\ sensitivity\ \% = 10.46 e^{-0.03072 (T)} \tag{8}$$

From Fig. 7 and Eq. (8) we can be seen the detrimental effect of temperature raise of pipe wall on the sensor sensitivity.

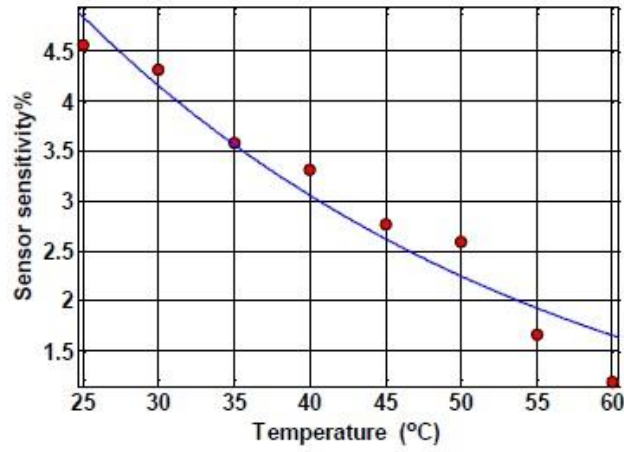


Fig. 7 Capacitance sensor sensitivity versus Temperature (°C)

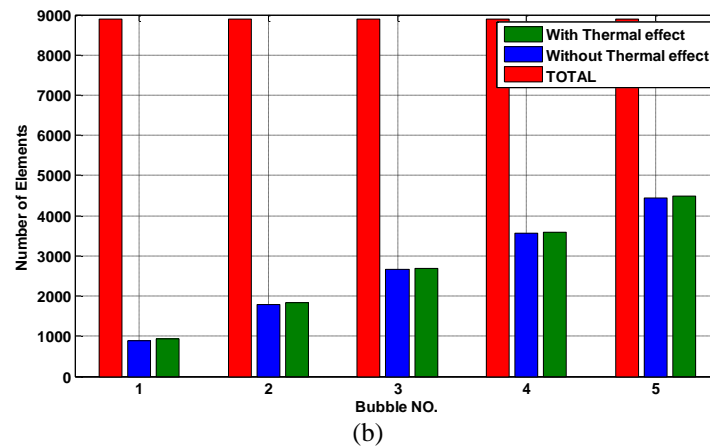
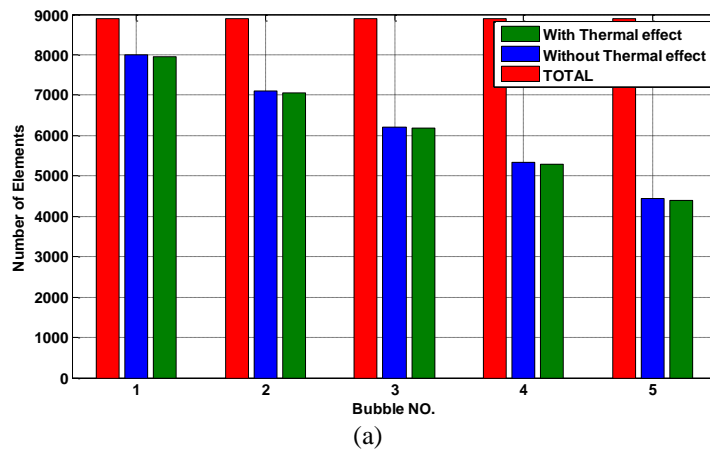


Fig. 8 (a) The water distribution across pipe at room temperature and with thermal effect and (b) The Air distribution across pipe at room temperature and with thermal effect

4.2 Calculation of void fraction distributions

Using the scripting capabilities in ANSYS simulation in Air–Water two-phase flow plotting by finite element analysis, we can be calculated the void fraction ($V_f\%$) at any time (t) at room temperature and with thermal effect by Eq. (9)

$$\left(V_f\% = \frac{\text{the number of element of air}}{\text{total number of element}} \times 100 \right) \tag{9}$$

Figs. 8(a), 8(b), 9(a), 9(b) represent the water/Air distribution and the void fraction $V_f\%$ distribution respectively at room temperature and with take the thermal effect.

From Fig. 9(b) we can be observed that the error % of the void fraction ($V_f\%$) due to thermal effect decrease when the bubble size increases, this is due to the fact that the change in the dielectric properties between air-water two-phase flow.

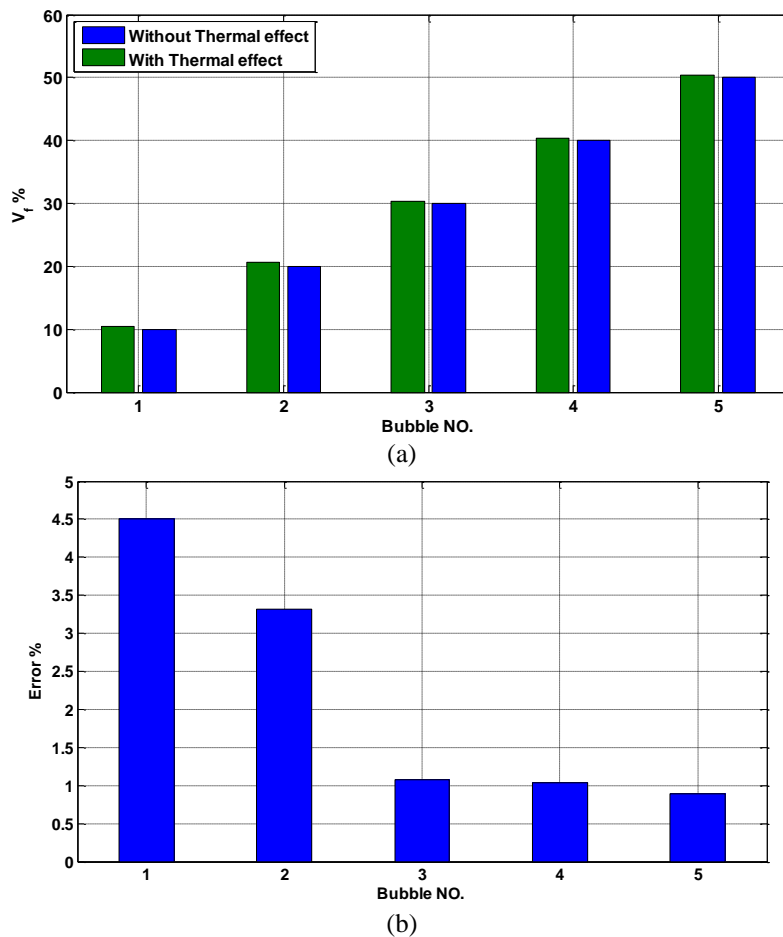


Fig. 9 (a) The void fraction $V_f\%$ distribution at room temperature and with thermal effect and (b) The Air void fraction distribution error due to thermal effect

5. Conclusions

This paper study a new factor has a great influence and effect on ECS sensitivity and sensitive domain of ECS electrodes, in order to increase the accuracy of two-phase flow measurements. The effect of temperature raise (T) of pipe wall on ECS was simulated using the forward 2D ANSYS model and the capacitance variations due to percentage changes of two phases were measured, and in addition the void fraction ($V_f\%$) was estimated at both room temperature and with take the thermal effect and the error between them was calculated. The concluded points emerged in this work can be summarized as follows:

1. The effect of the increase temperature of pipe wall is decrease of the maximum value of node potential of the electrodes and the capacitance values i.e., decrease the ability of the electrodes sensitivity and the sensitive domain of ECS electrodes.
2. The error % of the void fraction ($V_f\%$) due to thermal effect were found to be depend on the bubble size, as the bubble size increases the value of void fraction ($V_f\%$) error % decrease (see Fig. 9), this is due to the fact that the change in the dielectric properties between air-water two-phase flow.
3. The simulation results show a sensor sensitivity varied between 4.569 and 1.19% for temperature (T) ranging between 25 and 60°C for selected sensor geometrical parameters.
4. The FE model results have been verified using an experimental result available in the literatures. A good agreement was observed with an experimental result with an average error of 0.925%, as shown in Fig. 6, thus validating the accuracy and reliability of the proposed study.

References

- Al-Tabey, W.A. (2010), "Effect of pipeline filling material on electrical capacitance tomography", *Proceedings of the International Postgraduate Conference on Engineering (IPCE 2010)*, Perlis, Malaysia, October 16-17.
- Al-Tabey, W.A. (2012), *Finite Element Analysis in Mechanical Design Using ANSYS: Finite Element Analysis (FEA) Hand Book For Mechanical Engineers With ANSYS Tutorials*, LAP Lambert Academic Publishing, Germany, ISBN 978-3-8454-0479-0.
- Alme, K.J. and Mylvaganam, S. (2006), "Analyzing 3D and conductivity effects in electrical tomography systems using COMSOL multiphysics EM module", *Proceedings of the 2006 Nordic COMSOL Conference*.
- Altabay, W.A. (2016), "FE and ANN model of ECS to simulate the pipelines suffer from internal corrosion", *Struct. Monit. Maint.*, **3**(3), 297-314, DOI: <http://dx.doi.org/10.12989/smm.2016.3.3.297>.
- ANSYS Low-Frequency Electromagnetic analysis Guide, The Electrostatic Module in the Electromagnetic subsection of ANSYS, (2014), ANSYS, inc. Southpointe 275 Technology Drive Canonsburg, PA 15317, Published in the USA.
- Asencio, K., Bramer-Escamilla, W., Gutiérrez, G. and Sánchez, I. (2015), "Electrical capacitance sensor array to measure density profiles of a vibrated granular bed", *Powder Technol.*, **270**, 10-19.
- Banerjee, S. and Lahey, R.T. (1981), "Advances in two-phase flow instrumentation", *Adv. Nuclear Sci. Technol.*, **13**, 227-414.
- Couthard, J. and Yan, Y. (1993), "Ultrasonic cross-correlation flowmeter", *Measurement and Control*, **26**.
- Daoye, Y., Bin, Z., Chuanlong, X., Guanghua, T. and Shimin, W. (2009), "Effect of pipeline thickness on electrical capacitance tomography", *Proceedings of the 6th International Symposium on Measurement Techniques for Multiphase Flows, J. Phys. Conference Series*, **147**, 1-13.

- Fasching, G.E. and Smith, N.S. (1988), "High resolution capacitance imaging system", US Dept. Energy, **37**, DOE/METC-88/4083
- Fasching, G.E. and Smith, N.S. (1991), "A capacitive system for 3-dimensional imaging of fluidized-beds", *Rev. Sci. Instr.*, **62**, 2243-2251
- Hetsroni, G. (1982), "Hand book of Multiphase Systems", Hemisphere Publishing Corporation and McGraw-Hill, New York.
- Huang, S.M., Plaskowski, A.B., Xie, C.G. and Beck, M.S. (1989), "Tomographic imaging of two-flow component flow using capacitance sensor", *J. Phys. E : Sci. Instrum.*, **22**, 173-177.
- Jaworski, A.J. and Bolton, G.T. (2000), "The design of an electrical capacitance tomography sensor for use with media of high dielectric permittivity", *Meas. Sci. Technol.*, **11**(6), 743-757.
- Kumar, R.A., Cook, R.L., Norton, O.P. and Okhaysen, W.O. (1995), "Laser based cross-correlation technique for the determination of flow velocities in multiphase flows", *Proceedings of 1st International Symposium on Measurement Techniques for Multiphase Flows*, Nanjing, P.R. China.
- Li, H. and Huang, Z. (2000), "Special measurement technology and application", Zhejiang University Press, Hangzhou.
- Lynch, G.F. and Segal, S.L. (1977), "Direct measurement of the void fraction of a two-phase fluid by nuclear magnetic resonance", *Int. J. Mass Transfer*, **20**, 7-14.
- Mohamad, E.J., Rahim, R.A., Leow, P.L., Fazalul, Rahiman, M.H., Marwah, O.M.F., Nor Ayob, N.M., Rahim, H.A. and Mohd Yunus, F.R. (2012), "An introduction of two differential excitation potentials technique in electrical capacitance tomography", *Sensor. Actuat. A*, **180**, 1-10
- Mohamad, E.J., Rahim, R.A., Rahiman, M.H.F., Ameran, H.L.M., Muji, S.Z.M. and Marwah, O.M.F. (2016), "Measurement and analysis of water/oil multiphase flow using electrical capacitance tomography sensor", *Flow Meas. Instrum.*, **47**, 62-70.
- Pei, T. and Wang, W. (2009), "Simulation analysis of sensitivity for electrical capacitance tomography", *Proceedings of the 9th International Conference on Electronic Measurement & Instruments (ICEMI 2009)*.
- Sardeshpande, M.V., Harinarayan, S. and Ranade, V.V. (2015), "Void fraction measurement using electrical capacitance tomography and high speed photography", *J. Chem. Eng. Res. Des.*, **9**(4), 1-11.
- Thorn, R., Johansen, G.A. and Hammer, E.A. (1997), "Recent developments in three-phase flow measurement", *Meas. Sci. Technol.*, **8**, 691-701.
- Thorn, R., Johansen, G.A. and Hammer, E.A. (1999), "Three-phase flow measurement in the offshore oil industry—is there a place for process tomography?", *Proceedings of the 1st World Congress on Industrial Process Tomography*, Buxton, UK.
- Xie, C.G., Huang, S.M., Hoyle, B.S., Thorn, R., Lenn, C., Snowden, D. and Beck, M.S. (1992), "Electrical capacitance tomography for flow imaging: system model for development of image reconstruction algorithms and design of primary sensors", *IEEE Proceedings-G*, **139**(1), 89-98.
- Yang, W.Q. (1997), "Modelling of capacitance sensor", *IEEE proceedings: Measurement Science and Technology*, **144**(5), 203-208.
- Yang, W.Q. and York, T.A., (1999), "New AC-based capacitance tomography system", *IEEE proceedings: Measurement Science and Technology*, **146**(1), 47-53.
- Yang, W.Q., Beck, M.S. and Byars, M. (1995b), "Electrical capacitance tomography –from design to applications", *Measure. Control*, **28**(9), 261-266
- Yang, W.Q., Stott, A.L., Beck, M.S. and Xie, C.G. (1995a), "Development of capacitance tomographic imaging systems for oil pipeline measurements", *Rev. Sci. Instrum.*, **66**(8), 4326
- Zhang, W., Wang, C., Yang, W. and Wang, C. (2014), "Application of electrical capacitance tomography in particulate process measurement – A review", *J. Adv. Powder Technol.*, **25**, 174-188.